

Curvature profiles as initial conditions for primordial black hole formation

Alexander G. Polnarev, Ilia Musco

Astronomy Unit, Queen Mary University of London, Mile End Road, London E1 4NS, England

Abstract. This work is part of an ongoing research programme to study possible Primordial Black Hole (PBH) formation in the early universe. Working within spherical symmetry, we specify an initial configuration in terms of a curvature profile $K(r)$, which represents initial conditions for the large amplitude metric perturbations away from the homogeneous Friedmann Robertson Walker model which are required for PBH formation. This curvature profile $K(r)$ is directly linked to the time-independent co-moving curvature perturbation \mathcal{R} . Using an asymptotic quasi-homogeneous solution, we relate $K(r)$ with the density and velocity fields, which at a small enough initial time, when the length scale of the configuration is much larger than the cosmological horizon, can be treated as small perturbations of the background values. We present general analytic solutions for the density and velocity profiles. These solutions enable us to consider in a self-consistent way the formation of PBHs in A wide variety of cosmological situations with the cosmological fluid being presented as an arbitrary mixture of different components with different equations of state. We show that the analytical solutions for the density and velocity profiles as functions of the initial moment of time are similar to those for pure growing modes in standard cosmological perturbation theory. We then use two different parametrisation for $K(r)$ to follow the evolution of the initial configuration numerically, restricting attention to the formation of PBHs in the radiation dominated era.

26 October 2019

1. Introduction

The possible existence of primordial black holes (PBHs) was first proposed in 1966 by Zeldovich & Novikov [1] and, at the beginning of 1970s, by Hawking [2]. In the following years it was then widely discussed, see for example the recent review by Carr for a full list of references [3]. In 1974 Hawking made his famous discovery of black hole evaporation [4], that is cosmologically relevant if the mass of black holes is less than 10^{15} grams, as it possible to obtain only in the PBH scenario. For this reason the problem of PBH formation started to be attractive and have been widely investigated in the following 30 years.

The formation was first investigated by Carr (1975) [5] using a simplified model of an overdense collapsing region, described as a closed Friedmann-Robertson-Walker (FRW) universe, surrounded by a spatially flat FRW expanding background. In the radiation dominated epoch of the Universe this leads to a threshold value for the perturbation amplitude of $\delta_c \sim 1/3$, where the amplitude δ is defined as the mass excess in the overdensity region, and black holes formed had masses of the order of the horizon mass at the time of formation. This estimation of δ_c is just a rough estimate

obtained comparing the Jeans length with the cosmological horizon length at the time of black hole formation. Subsequently self consistent hydrodynamical analysis of PBH formation have been carried out by Nadezhin, Novikov and Polnarev in 1978 [6] using, for the first time in this context, an hydrodynamical computer code written in the Misner-Sharp slicing, characterised by a diagonal metric with a cosmic time coordinate, that reduces to the FRW metric in absence of perturbations. The same slicing was used by May & White [7] and Podurets [8] to study stellar collapse, with the fundamental difference in Nadezhin *et al* of introducing for the first time an early form of excision to avoid the problem of singularity formation. An equivalent analysis was then developed in 1979 by Bicknell & Henriksen [9] using a different method based on integration along hydrodynamical characteristics. These works showed that the threshold amplitude of the perturbation is dependent on the particular shape of the initial conditions. It was also found that the pressure gradients reduce considerably the PBH mass formed at the end of the hydrodynamical process as was clearly pointed out by Nadezhin *et al* [6] (They obtained black hole masses down to 10^{-2} the horizon mass calculated at the time of formation). They showed also that the black hole formation can lead to the production of compression waves and shocks, as was also observed in the equivalent simulations performed by Bicknell & Henriksen [9].

In the following twenty years no other numerical studies were made on the formation mechanism and attention was concentrated on different aspects. For example there was consideration of the amount of Hawking radiation emitted by sufficiently small PBHs, with a mass less than 10^{15} g, to obtain important constraints on parameters that characterise the different epochs and process of the Universe [10]. The formation of PBHs was considered also in different scenarios: during phase transitions [11], with a soft equation of state [12], as collapse of cosmic loops and domain walls [13] or from bubble collisions [14]. In general the study of PBHs provides a unique probe for different areas of physics: the early Universe, quantum gravity, gravitational collapse and high energy physics. This is explained with full list of references in different reviews of PBHs, as for example [3].

Recently, in 1999, Niemeyer and Jedamzik have made new numerical calculations pointing out the relevance of scaling law for PBH formation. They showed [15, 16] that the black hole mass M_{BH} follows the power law in $(\delta - \delta_c)$ if δ is close enough to δ_c , the same behaviour seen in critical collapse by Choptuik [17] and other authors (see the review of Gundlach [18]). Niemeyer and Jedamzik found at horizon crossing $\delta_c \simeq 0.7$ for the three types of perturbation profile that they studied. In the same year Shibata and Sasaki [19] presented an alternative formalism for studying PBH formation focusing on metric perturbations rather than density perturbations, as was done also in the past [6, 20]. They pointed out that the initial conditions used in [16] were specified initially within non linear regime of perturbations of the energy density and velocity field, and were therefore “inevitably contaminated by an unrealistic decaying mode” component that would diverge for $t \rightarrow 0$. In a recent paper [21] this analyses have been converted into the common formalism of perturbation amplitude δ , showing that the Shibata and Sasaki results, correspondent to a wide choice of perturbation shapes, are consistent with a value of δ_c in the range $0.3 \lesssim \delta_c \lesssim 0.5$.

The disagreement between this and the value $\delta_c \simeq 0.7$ has been explained by Musco *et al* [22] where similar simulations to those of Niemeyer & Jedamzik were carried out with the improvement of specifying the initial conditions within the linear regime, giving only growing mode solution at the horizon crossing time. Their simulations give corresponding values of δ_c in the range $0.43 - 0.47$ (instead of

0.67 – 0.71) for the same types of perturbation profile used by Niemeyer and Jedamzik in [16].

The present work is a new development of the analysis of PBHs using the numerical technique used by Musco *et al* [22], using a quasi homogeneous solution characterised by a curvature profile to specify the initial conditions. This is a further evolution of the original idea of Nadezhin *et al* [6]. We will not discuss again in detail the procedure used for calculating the numerical evolution, just described in [22], but give just a very brief description in sub-sections 2.1 of the Misner-Sharp equations that then are used in sub-section 2.2 as the context within which to impose the initial conditions as function of a curvature profile, showing that the regime of a quasi homogeneous solution correspond to the regime when length scale of the perturbation is much larger than the cosmological horizon. Then in sub-section 2.3 we discuss the dependence of the solution on the particular choice of the equation of state, correspondent to a cosmological fluid characterised by a mixture of different components. In section 3 we discuss in the first subsection the physical properties of the curvature profile $K(r)$, while in the second one we show that the perturbations that we are using are equivalent to the pure growing modes of the cosmological perturbation theory. We show also that the curvature profile $K(r)$ is also directly connected to the time-independent comoving curvature perturbation \mathcal{R} . In section 4 we explain how a particular parametrisation of the curvature profile have been introduced into the numerical scheme, using explicitly two different parametrisation of $K(r)$ as examples. Finally in section 5 we first calculate with numerical tests how to impose consistently into the code initial conditions described by the quasi homogeneous solution, giving then numerical examples of primordial black hole formation in the representative case of a radiation dominated universe. We show how the threshold for black hole formation is linked with the curvature profile and discuss the results obtained with the two different parametrisation used. Summary and conclusions are the given in section 6.

2. Mathematical formulation of the problem

Subsection 2.1 summarises the Misner-Sharp set of equations, based on the cosmic time formulation, while subsection 2.2 introduces the curvature perturbation in this set of equations and shows how the hydrodynamic quantities depend on it. Finally subsection 2.3 shows how the general solution is related to the choice of the equation of state, generalised here to describe the cosmological fluid as a mixture of different perfect fluid components.

2.1. The Misner-Sharp equations

For calculations in spherical symmetry, it is convenient to divide the collapsing matter into a system of concentric spherical shells and to label each shell with a Lagrangian co-moving radial coordinate which we will denote with r . The metric can then be written in the form

$$ds^2 = -a^2 dt^2 + b^2 dr^2 + R^2 (d\theta^2 + \sin^2 \theta d\varphi^2), \quad (1)$$

where R (the Schwarzschild circumference coordinate), a and b are functions of r and the time coordinate t . This was the form used Misner & Sharp (1966) [23].

For a classical fluid, composed of particles with nonzero rest-mass, it is convenient to use the rest-mass μ contained interior to the surface of a shell (or, equivalently,

the baryon number) as its co-moving coordinate r . For fluids not possessing these conserved quantities, one can still define a “relative compression factor” ρ [24, 25] (equivalent to the rest-mass density in the standard treatment) and one then has

$$d\mu = 4\pi\rho R^2 b dr. \quad (2)$$

Identifying μ and r then gives

$$b = \frac{1}{4\pi R^2 \rho}. \quad (3)$$

Following the notation of [23], we write the equations in terms of the operators

$$D_t \equiv \frac{1}{a} \left(\frac{\partial}{\partial t} \right), \quad (4)$$

$$D_r \equiv \frac{1}{b} \left(\frac{\partial}{\partial \mu} \right), \quad (5)$$

and applying these to R gives

$$D_t R \equiv U, \quad (6)$$

$$D_r R \equiv \Gamma, \quad (7)$$

where U is the radial component of the four-velocity in the associated Eulerian frame, using R as the radial coordinate, and Γ is a generalisation of the Lorentz factor.

We are mostly dealing here with processes where the matter can be well described by a perfect fluid and the equation of state of the matter can be written as

$$p = \gamma e, \quad (8)$$

where p is the pressure and e is the energy density (note that this γ is not the adiabatic index). For one-parameter equations of state of the form $p = p(e)$, the system of Einstein and hydrodynamic equations can be written as:

$$D_t U = - \left[\frac{\Gamma}{(e+p)} D_r p + \frac{M}{R^2} + 4\pi R p \right], \quad (9)$$

$$D_t \rho = - \frac{\rho}{\Gamma R^2} D_r (R^2 U), \quad (10)$$

$$D_t e = \frac{e+p}{\rho} D_t \rho, \quad (11)$$

$$D_r a = - \frac{a}{e+p} D_r p, \quad (12)$$

$$D_r M = 4\pi \Gamma e R^2, \quad (13)$$

where M is a measure of the mass-energy contained inside radius μ and Γ can be calculated either from (7) or from the constraint equation

$$\Gamma^2 = 1 + U^2 - \frac{2M}{R}. \quad (14)$$

When using the time slicing of the metric (1) for studying collapse leading to black hole some problems are encountered, given by formation of singularities that appear before the interesting parts of the evolution have been completed, terminating the calculation. There are various ways of remedying this. Hernandez & Misner [26] introduced the concept of “observer time”, using as the time coordinate the

time at which an outgoing radial light ray emanating from an event reaches a distant observer. In the original formulation, this observer was placed at future null infinity but for calculations in an expanding cosmological background we use an FRW fundamental observer sufficiently far from the perturbed region to be unaffected by the perturbation. A complete description of the Misner-Hernandez equations is given in [22].

2.2. Introducing a Curvature perturbation

Next we will rewrite the Misner-Sharp equations in terms of a quasi homogeneous solution which allows to give a non perturbative description of large amplitude metric perturbations away from the homogeneous FRW model. We know infact that only these large perturbations will be able to give rise to PBH formation, and using this approach we will be able to avoid the arbitrariness in the choice of initial conditions considered in the previous works [15, 19, 22]. In this scenario infact the perturbations predicted by any cosmological model are relevant only when one calculates the probability of finding large amplitude perturbations of the metric.

The amplitude of the energy density perturbations arising in the early universe is initially very small and therefore the Einstein equations should have a quasi homogeneous solution. The characteristic feature of this solution is that near the singularity all mass elements expand with the solution of the FRW model ($e = 1/6(1 + \gamma)^2 \pi t$ for an equation of state given by (8)). However a spatial hypersurface with $t = \text{const}$ can have an arbitrarily curvature if it is defined on a sufficiently large scale. Therefore, according with this solution, any hydrodynamical quantity as energy and pressure, can be considered in the asymptotic regime ($t \rightarrow 0$), as slight perturbed with respect the homogeneous solution. This asymptotic regime correspond to an initial scale of the perturbation much larger than the initial cosmological horizon. In other words we know that a generic curvature perturbation has a corresponding density perturbation and that, when the length scale of the perturbation is much larger than the horizon scale, the curvature perturbation is time independent, because pressure gradients are negligible [28, 27] and therefore the correspondent density and velocity field perturbation are just small deviation with respect the homogeneous solution. It is therefore convenient to use this approach to describe the perturbations will lead to the formation of PBHs.

In this work, using spherical symmetry, we specify the initial condition on the spatial hypersurface using a time independent function $K = K(r)$ that represent the curvature profile and, how we will see in the next section, is directly related to the comoving curvature perturbation \mathcal{R} . We can also see that introducing a profile $K(r)$ into the Friedmann Robertson Walker metric, this is an asymptotic solution of the Einstein equation in the limit $t \rightarrow 0$. Therefore, using $K(r)$ to represent the curvature perturbation for perturbations with scales much larger than the horizon length, we need to solve the system of perturbed differential equations in order to calculate how the set of variables depends on $K(r)$ in this regime.

To develop the perturbative analysis of all the quantities appearing in the Misner-Sharp equations we need to solve the following system of differential equations:

$$\dot{R} = aU \tag{15}$$

$$\frac{\dot{b}}{b} = a \frac{U'}{R'} \tag{16}$$

$$\frac{a'}{a} = -\frac{\gamma}{1+\gamma} \frac{e'}{e} \quad (17)$$

$$\dot{M} = -4\pi\gamma e R^2 \dot{R} \quad (18)$$

$$M' = 4\pi e R^2 R' \quad (19)$$

$$\frac{R'^2}{b^2} = 1 + U^2 + \frac{2M}{R} \quad (20)$$

where the dot and dash denote differentiation with respect to t and r respectively, and we have used the equation of state (8) to express pressure as function of energy density, (7) to give an expression for Γ , and ρ can be calculated later with equation (10).

In general we will present analytical solutions for an arbitrary parameter $\gamma = \gamma(t)$ that describes the universe as a general mixture of different components with constant γ as dust ($\gamma = 0$), radiation ($\gamma = 1/3$) and “dark energy” ($\gamma < -1/3$). Later we present some numerical examples characterised by the simplest case of one fluid component described by $\gamma = 1/3$.

The background value of the energy density (indicated with the suffix “b”) is calculated with the Friedmann equation

$$\left(\frac{\dot{s}}{s}\right)^2 = H_b^2 = \frac{8\pi}{3} e_b, \quad (21)$$

while the background value of the other quantities is derived from the FRW metric and above the set of equations (15 - 20).

$$a_b = 1 \quad (22)$$

$$b_b = s(t) \quad (23)$$

$$R_b = s(t)r \quad (24)$$

$$M_b = \frac{4}{3}\pi e_b R_b^3 \quad (25)$$

$$U_b = H_b R_b = \dot{s}(t)r \quad (26)$$

As we have explained before, when the perturbation is well outside the cosmological horizon all the hydrodynamical quantities can be treated as being nearly homogeneous, making the perturbations of the hydrodynamical quantities small deviations with respect to the uniform solution. It is useful therefore to parametrise the scale of the perturbations using a dimensionless parameter ϵ that shows explicitly the ratio between the physical length scale of the perturbation $R_0 = s(t)r_0$ and the horizon scale $R_H = H_b^{-1}$.

$$\epsilon \equiv \left(\frac{R_H}{R_0}\right)^2 = \left(\frac{1}{H_b s r_0}\right)^2 = \frac{1}{\dot{s}^2 r_0^2} \ll 1 \quad (27)$$

By definition, ϵ is related only to the background quantities and therefore is only a function of time, with the behaviour of its time derivative being given by

$$\frac{\dot{\epsilon}}{\epsilon} = -2\frac{\dot{s}}{s} - \frac{\dot{e}_b}{e_b} = -2\frac{\dot{s}}{s} + 3(1+\gamma)\frac{\dot{s}}{s} = (1+3\gamma)\frac{\dot{s}}{s}, \quad (28)$$

$$\xi \equiv \ln(s), \quad \frac{s}{\dot{s}} \frac{\partial}{\partial t} \equiv \frac{\partial}{\partial \xi}, \quad \frac{\partial}{\partial r} \equiv \left(\frac{\partial}{\partial r}\right)'. \quad (29)$$

In particular it is important to point out that expression (28) is a consequence of energy conservation law and that it holds also when γ is a general function of time.

We treat ϵ as a small parameter in the asymptotic solution and we will see that it will not appear in any final equation of this section. However, when we will present the numerical implementation of this formalism, we will need to calculate explicitly a value of ϵ that will ensure the consistency of the quasi homogeneous solution into the numerical scheme. Initially the perturbation of each quantity is defined as:

$$R = R_b(1 + \epsilon\tilde{R}) \quad (30)$$

$$U = H_b R(1 + \epsilon\tilde{U}) \quad (31)$$

$$b = \frac{R'}{\sqrt{1 - K(r)r^2}}(1 + \epsilon\tilde{b}) \quad (32)$$

$$a = 1 + \epsilon\tilde{a} \quad (33)$$

$$e = e_b(1 + \epsilon\tilde{e}) \quad (34)$$

$$M = \frac{4}{3}\pi e_b R^3(1 + \epsilon\tilde{M}) \quad (35)$$

If the value of ϵ is small enough we can neglect high order terms in the perturbative expressions of the hydrodynamical equations (15-20).

Starting from equation (15), and using expressions (28) and (29) we get,

$$\frac{\dot{s}}{s} + (\epsilon\tilde{R})^\cdot = \frac{\dot{s}}{s}(1 + \epsilon\tilde{a})(1 + \epsilon\tilde{U})$$

hence

$$(1 + 3\gamma)\tilde{R} + \frac{\partial\tilde{R}}{\partial\xi} = \tilde{a} + \tilde{U}. \quad (36)$$

Perturbing equation (16) we get

$$(\epsilon\tilde{b})^\cdot = -\frac{a'U}{R'}$$

which gives

$$(1 + 3\gamma)\tilde{b} + \frac{\partial\tilde{b}}{\partial\xi} = -r\tilde{a}'. \quad (37)$$

Perturbing equation (17) and integrating it over r we have

$$(1 + \gamma)\tilde{a} + \gamma\tilde{e} = 0. \quad (38)$$

Perturbing equation (18) we get

$$\frac{1}{3}(1 + \epsilon\tilde{M}) \left[\frac{\dot{e}_b}{e_b} + 3\frac{\dot{R}}{R} + (\epsilon\tilde{M})^\cdot \right] = \gamma(1 + \epsilon\tilde{e})\frac{\dot{R}}{R},$$

that, using (28), we can write as

$$\begin{aligned} \frac{\dot{e}_b}{e_b} &= -3(1 + \gamma)\frac{\dot{s}}{s} \\ &- 3(1 + \gamma)\frac{\dot{s}}{s} + 3(1 + \gamma)\frac{\dot{R}}{R} - 3(1 + \gamma)\frac{\dot{s}}{s}\epsilon\tilde{M} + (\epsilon\tilde{M})^\cdot + \\ &+ 3\frac{\dot{s}}{s}\epsilon\tilde{M} + 3\gamma\frac{\dot{R}}{R}\epsilon\tilde{e} = 0. \end{aligned}$$

Using now equation (15) we get some simplifications

$$\dot{\epsilon}\tilde{M} + \epsilon\dot{\tilde{M}} - 3\gamma\frac{\dot{s}}{s}\epsilon\tilde{M} + 3\gamma\frac{\dot{s}}{s}\epsilon\tilde{e} + 3(1+\gamma)(\dot{\epsilon}\tilde{R} + \epsilon\dot{\tilde{R}}) = 0,$$

and finally using equation (36) and (38) we get

$$\tilde{M} + \frac{\partial\tilde{M}}{\partial\xi} = -3(1+\gamma)\tilde{U}. \quad (39)$$

Perturbing equation (19) we get

$$\frac{1}{3}(1+\epsilon\tilde{M}) \left[3\frac{R'}{R} + (\epsilon\tilde{e}') \right] = (1+\epsilon\tilde{e})\frac{R'}{R},$$

that after some algebra can be written as

$$\tilde{e} = \frac{1}{3r^2}(r^3\tilde{M})'. \quad (40)$$

Finally, perturbing equation (20), we have

$$\left[(1 - K(r)r^2)(1 - 2\epsilon\tilde{b}) - 1 \right] = \frac{\dot{s}^2}{s^2}R^2(1 + 2\epsilon\tilde{U}) - \frac{8\pi e_b R^3}{3R}(1 + \epsilon\tilde{M}),$$

that using (21) becomes

$$- \left[K(r)r^2 + 2\epsilon\tilde{b}(1 - K(r)r^2) \right] = R^2\frac{\dot{s}^2}{s^2}\epsilon(2\tilde{U} - \tilde{M}),$$

and now using expression (27) for ϵ we have

$$- \left[K(r)r^2 + 2\epsilon\tilde{b}(1 - K(r)r^2) \right] = \frac{r^2}{r_0^2}(2\tilde{U} - \tilde{M}). \quad (41)$$

At this point we use the approximation of considering perturbations with length-scales larger than the horizon ($\epsilon \ll 1$) that allows the higher order term to be neglected, giving

$$\tilde{U} = \frac{1}{2} \left[\tilde{M} - K(r)r_0^2 \right]. \quad (42)$$

This is the only equation of the system where, at the end of the algebra, $K(r)$ is appearing explicitly. From the definition of Γ given in (7) one can rewrite (42) as

$$K(r) = \frac{1 - \Gamma^2}{r^2}. \quad (43)$$

which is a useful expression to study later the order of this approximation as a function of ϵ . This relation shows also the connection between the profile $K(r)$ and Γ , which is an invariantly defined quantity representing an energy per unit mass.

Now we can solve the system of perturbative equations composed of the four differential equations (37, 36, 39, 40), and two algebraic equations (38, 42). Substituting (42) into equation (39) we get

$$\frac{\partial\tilde{M}}{\partial\xi} + \frac{5+3\gamma}{2}\tilde{M} = \frac{3}{2}(1+\gamma)K(r)r_0^2, \quad (44)$$

and from this expression we can see that it is possible to separate the variables (r, ξ) because, as we have assumed at the beginning, γ is just a function of time related to the homogeneous solution. We therefore write

$$\tilde{M} = \Phi(\xi)K(r)r_0^2, \quad (45)$$

that gives the following differential equation for the function $\Phi(\xi)$

$$\frac{d\Phi}{d\xi} + \frac{5+3\gamma}{2}\Phi = \frac{3}{2}(1+\gamma). \quad (46)$$

Before entering into a detailed discussion of the particular equation of state, we treat for the moment $\Phi(\xi)$ as a general function of time and solve the system of perturbed equations. Expression (45) is the solution for the mass perturbation \tilde{M} and inserting this into (40) and subsequently making all of the consequent substitutions in (38) and (42) we get the general expression for the energy density perturbation \tilde{e} , lapse perturbation \tilde{a} and radial velocity perturbation \tilde{U} :

$$\tilde{e} = \Phi(\xi) \frac{1}{3r^2} [r^3 K(r)]' r_0^2 \quad (47)$$

$$\tilde{a} = -\Phi(\xi) \frac{\gamma}{1+\gamma} \frac{1}{3r^2} [r^3 K(r)]' r_0^2 \quad (48)$$

$$\tilde{U} = \frac{1}{2} [\Phi(\xi) - 1] K(r) r_0^2 \quad (49)$$

Substituting these solutions into (36) and (37) we find two differential equations for the perturbation quantities \tilde{R} and \tilde{b} , given by

$$(1+3\gamma)\tilde{R} + \frac{\partial \tilde{R}}{\partial \xi} = -\Phi(\xi) \frac{\gamma}{1+\gamma} \frac{1}{3r^2} [r^3 K(r)]' r_0^2 + \frac{1}{2} [\Phi(\xi) - 1] K(r) r_0^2, \quad (50)$$

$$(1+3\gamma)\tilde{b} + \frac{\partial \tilde{b}}{\partial \xi} = \frac{\gamma}{(1+\gamma)} r \left[\frac{1}{3r^2} [r^3 K(r)]' \right]' \Phi(\xi), \quad (51)$$

that can be solved introducing two new functions of time $I_1(\xi)$ and $I_2(\xi)$ related to $\Phi(\xi)$ as follows

$$\tilde{R} = -I_1(\xi) \frac{1}{3r^2} [r^3 K(r)]' r_0^2 + I_2(\xi) \frac{K(r)}{2} r_0^2, \quad (52)$$

$$\tilde{b} = I_1(\xi) r \left[\frac{1}{3r^2} (r^3 K(r))' \right]' r_0^2. \quad (53)$$

The relation between $I_{1,2}(\xi)$ and $\Phi(\xi)$ is obtained introducing (52) and (53) into (50) and (51).

$$\frac{dI_1(\xi)}{d\xi} + (1+3\gamma)I_1(\xi) = \frac{\gamma}{1+\gamma}\Phi(\xi) \quad (54)$$

$$\frac{dI_2(\xi)}{d\xi} + (1+3\gamma)I_2(\xi) = [\Phi(\xi) - 1] \quad (55)$$

This completes the general solution of the system of equations that is formed by expressions (45), (47), (48), (49), (52), (53) for the set of perturbations and by the first order differential equations (46), (54), (55) for these functions. It is interesting to observe the form of this solution, with the separation between the time evolution given by ϵ and Φ , and the space dependence given by $K(r)$.

2.3. Explicit form of the time functions

Now we discuss the nature of the functions Φ , I_1 , I_2 and understand explicitly how they are related to the homogeneous solution. In general the universe consists of different

fluid components characterised by different constant values γ_i . Therefore the function γ can be treated as a general function of time, defined as

$$\gamma(s) \equiv \frac{\sum_i p_i}{\sum_i e_i} = \frac{\sum_i \gamma_i e_i}{\sum_i e_i} = \frac{\sum_i \gamma_i e_i}{e}. \quad (56)$$

At the initial time it is possible to express the presence of each component in the universe determining the fractional amount f_i with the correspondent coefficient γ_i , having for each component

$$e_i = f_i e \sim s^{-3(1+\gamma_i)}, \quad \sum_i f_i = 1, \quad (57)$$

where f_i and γ_i are constants. Therefore

$$\gamma = \frac{\sum_i f_i \gamma_i s^{-3(1+\gamma_i)}}{\sum_i f_i s^{-3(1+\gamma_i)}} \quad (58)$$

$$Q(s) \equiv \sum_i f_i s^{-3(1+\gamma_i)} \sim e(s) \sim H^2(s) \quad (59)$$

$$\begin{aligned} s \frac{dQ}{ds} &= \frac{dQ}{d\xi} = -3 \sum_i f_i s^{-3(1+\gamma_i)} - 3 \sum_i \gamma_i f_i s^{-3(1+\gamma_i)} = -3Q - 3\gamma Q \\ \frac{dQ}{d\xi} &= -3(1+\gamma)Q \quad \text{or} \quad \frac{3(1+\gamma)}{2} = -\frac{1}{2} \frac{dQ}{Q d\xi} = -\frac{1}{H} \frac{dH}{d\xi} \end{aligned} \quad (60)$$

Using this last equation for γ in equation (46) one obtains

$$\frac{d\Phi}{d\xi} + \left(1 - \frac{1}{H} \frac{dH}{d\xi}\right) \Phi = -\frac{1}{H} \frac{dH}{d\xi},$$

and this equation can be solved with a general solution of the form

$$\Phi = F e^\mu.$$

After substitution, it is found that F and μ have to satisfy the following differential equations

$$\begin{aligned} \frac{dF}{d\xi} &= -\frac{1}{H} \frac{dH}{d\xi} e^{-\mu}, \\ \frac{d\mu}{d\xi} + 1 - \frac{1}{H} \frac{dH}{d\xi} &= 0, \end{aligned}$$

giving

$$e^{-\mu} = e^{\ln s - \ln H} = \frac{s}{H},$$

$$F = \frac{s}{H} - \int_0^s \frac{ds'}{H},$$

and finally

$$\Phi(s) = 1 - \frac{H(s)}{s} \int_0^s \frac{ds}{H(s)}. \quad (61)$$

Now we can solve the two differential equations for I_1 and I_2 that are both of the same form,

$$s \frac{I(s)}{ds} + (1 + 3\gamma)I(s) = F(s) \quad (62)$$

where $F(s) = \frac{\gamma(s)}{1+\gamma(s)}\Phi(s)$ in the case of $I(s) = I_1(s)$, while $F(s) = \Phi(s) - 1$ when $I(s) = I_2(s)$. From the expression (28) it is possible to write

$$1 + 3\gamma = \frac{1}{H\epsilon} \frac{d\epsilon}{dt} = H^2 s^2 \left(s \frac{d(1/H^2 s^2)}{ds} \right) \quad (63)$$

and this allows the differential equations (62) to be written in a form that can easily be integrated,

$$s \frac{d}{ds} \left[\frac{1}{H^2 s^2} I(s) \right] = \frac{1}{H^2 s^2} F(s) \quad (64)$$

therefore

$$I(s) = H^2(s) s^2 \int_0^s F(s) \frac{1}{H^2(s) s^2} \frac{ds}{s}, \quad (65)$$

which gives the following expressions for the two functions I_1 and I_2 :

$$I_1(s) = H^2(s) s^2 \int_0^s \frac{\gamma(s)}{1+\gamma(s)} \Phi(s) \frac{1}{H^2(s) s^2} \frac{ds}{s}, \quad (66)$$

$$I_2(s) = H^2(s) s^2 \int_0^s (\Phi(s) - 1) \frac{1}{H^2(s) s^2} \frac{ds}{s}. \quad (67)$$

All the physical quantities are now related in a general and consistent way with three fundamental degrees of freedom in the choice of initial conditions. The first one depends just on time and is given by the time functions $Q(s)$ or $H(s)$ that specify the various components of particles, scalar fields, cosmic strings, etc., present in the Universe at the particular time chosen for imposing the initial conditions. In other words the time functions $(\gamma(s), \epsilon(s), \Phi(s), I_1(s), I_2(s))$ contain the homogeneous history of the Universe, from the beginning until the time of imposing the initial conditions. The second degree of freedom depends just on space and is given by the particular profile chosen for the spatial curvature profile $K(r)$. The last degree of freedom is given by the choice of the initial perturbation scale with respect to the horizon scale, chosen such that $\epsilon \ll 1$ in order to make the perturbative analysis self-consistent.

In the second part of this paper, when we will consider some numerical examples of this formalism, we will concentrate on the simplest case for the equation of state, with $\gamma = \text{const} = 1/3$, because the radiation epoch of the universe is the standard scenario for PBH formation. This means that the Hubble parameter behaves as

$$H(s) \sim s^{-\frac{3(1+\gamma)}{2}}, \quad (68)$$

and the integrated functions Φ , I_1 , and I_2 are just constants

$$\Phi = \frac{3(1+\gamma)}{5+3\gamma} \quad (69)$$

$$I_1 = \frac{\gamma}{(1+3\gamma)(1+\gamma)} \Phi = \frac{3\gamma}{(1+3\gamma)(5+3\gamma)} \quad (70)$$

$$I_2 = \frac{1}{1+3\gamma} (\Phi - 1) = -\frac{2}{(1+3\gamma)(5+3\gamma)} \quad (71)$$

In this simple case, therefore, the tilda-quantities are time independent and the time evolution is determined just by ϵ . This allows us to reproduce easily the standard

solution of cosmological perturbation theory for growing mode perturbations when γ is a constant. From (28) we can calculate the time evolution of ϵ

$$\epsilon(t) = \epsilon(t_0) \left(\frac{t}{t_0} \right)^{\frac{2(1+3\gamma)}{3(1+\gamma)}}, \quad (72)$$

and this is exactly the standard solution of the perturbation equation [31, 27].

3. General properties of the curvature profile $K(r)$

3.1. Physical properties

One important aspect coming from the definition of b given by (32) is the mathematical requirement that the argument inside the square root must be positive,

$$1 - K(r)r^2 > 1 \quad \Rightarrow \quad K(r) < \frac{1}{r^2} \quad (73)$$

otherwise in the range of r where the argument of the square root is negative the comoving radius is not defined. This corresponds to the physical condition that a perturbed spherical region of comoving radius r should not already be causally disconnected from the rest of the Universe at early times. Another important property is the conservation of the total energy of the Universe, when the perturbation is made,

$$\int_0^\infty 4\pi r^2 \tilde{e}(r) dr = 0, \quad (74)$$

that implies

$$\lim_{r \rightarrow \infty} r^3 K(r) = 0, \quad (75)$$

which means also that the Universe remains spatially flat on a large enough scale. A final property of the profile of curvature is the value of r_0 that specifies the length-scale of the perturbation; from (47) we have

$$\tilde{e}(r_0) = 0 \quad \Rightarrow \quad K(r_0) + \frac{r_0}{3} K'(r_0) = 0. \quad (76)$$

It is useful to introduce an integrated quantity δ that measures the mass-excess inside the overdensity, as used frequently in the literature. From equation (40), one sees that any spherical integral of \tilde{e} is independent of the particular curvature profile used, but depends just on the value of $K(r)$ at the outer edge of the interval. The expression for δ is then given by

$$\delta \equiv \left(\frac{4}{3} \pi r_0^3 \right)^{-1} \int_0^{r_0} 4\pi \frac{e - e_b}{e_b} r^2 dr = \epsilon(s) \Phi(s) K(r_0) r_0^2, \quad (77)$$

and we can appreciate from this expression that δ is gauge independent since it is directly proportional to $K(r_0)r_0^2$, which is an invariantly defined quantity. We can appreciate the perfect separation of the different physical contributions: ϵ specifies the evolution of the perturbation amplitude in the long wavelength limit, Φ gives the contribution of the equation of state and $K(r_0)r_0^2$ specifies the spatial profile of the perturbation.

3.2. The curvature profile and the comoving curvature perturbation

Now we show how to link the curvature profile $K(r)$ to the comoving curvature perturbation \mathcal{R} [27]. The simplest definition of \mathcal{R} comes from a linear perturbation of the FRW metric (however it is possible to define an analogous quantity in general [29, 30]), where the spatial part of the metric tensor is given by

$$g_{ij} = s^2 [(1 + 2\mathcal{R}) \delta_{ij}] , \quad (78)$$

and the calculation of the spatial scalar curvature $R^{(3)}$ gives

$$R^{(3)} = 4 \frac{k^2}{s^2} \mathcal{R} , \quad (79)$$

where k is the comoving wavenumber associated with the perturbation. The comoving curvature perturbation \mathcal{R} is also connected with the pure growing mode solution of the perturbation equation for the energy density by

$$\frac{\delta e}{e_b} = \frac{2(1+\gamma)}{5+3\gamma} \left(\frac{k}{sH} \right)^2 \mathcal{R} . \quad (80)$$

This relation is obtained using a quantity called the “peculiar gravitational potential” Φ_G defined as

$$\frac{\delta e}{e_b} = -\frac{2}{3} \left(\frac{k}{sH} \right)^2 \Phi_G , \quad (81)$$

that is linked to \mathcal{R} with a first order differential equation

$$\frac{1}{H} \dot{\Phi}_G + \frac{5+3\gamma}{2} \Phi_G = -(1+\gamma) \mathcal{R} , \quad (82)$$

that has pure growing solution given by

$$\Phi_G = -\frac{3(1+\gamma)}{5+3\gamma} \mathcal{R} . \quad (83)$$

When the length-scale of a perturbation is much larger than the horizon scale, the pressure gradients are negligible and therefore it turns out that \mathcal{R} and Φ_G are time independent (This was shown first in 1963 by Lifshits & Khalamikov [28], and more recently by Lyth *et al* [29] and Langlois & Vernizzi [30]).

If we calculate the spatial scalar curvature (see appendix) with the curvature profile $K(r)$ explicitly written in the metric, we find that

$$R = 6 \left[\frac{\ddot{s}}{s} \left(1 + \epsilon \frac{3\gamma-1}{5+3\gamma} \mathcal{K} \right) + \frac{\dot{s}^2}{s^2} \left(1 - \epsilon \frac{2(2+3\gamma)}{5+3\gamma} \mathcal{K} \right) + \frac{\mathcal{K}}{s^2} \right] , \quad (84)$$

where

$$\mathcal{K} = K(r) + \frac{r}{3} K'(r) . \quad (85)$$

Because the metric is diagonal the spatial component is perpendicular to the time one and

$$R^{(3)} = \frac{6}{s^2} \left[K(r) + \frac{r}{3} K'(r) \right] . \quad (86)$$

If we identify $k = 1/r_0$, which is natural because the wave number is representing the inverse of the wavelength of the perturbation, we see that

$$\epsilon = \left(\frac{k}{sH} \right)^2 . \quad (87)$$

Using this and comparing equation (79) with (86) we see that the two equations are the same if we identify

$$\mathcal{R} = \frac{3}{2}r_0^2 \left[K(r) + \frac{r}{3}K'(r) \right] \quad (88)$$

and the same result is obtained comparing (47) with (80). We notice also that equation (82) is the same as (46), in fact the peculiar gravitational potential defined in (81) can be written in our terminology as $\Phi_G = -(2/3)\tilde{e}$ and then we can use equation (40) to express the variable \tilde{M} in terms of \tilde{e} in (46). We have therefore shown that \mathcal{R} is directly linked to $K(r)$.

4. Parametrisation of the curvature profile

In this section we make a particular choice for the profile of $K(r)$ in terms of two free parameters. We discuss this particular choice explaining how the curvature specification is inserted into the code and showing how the shapes of the perturbations are modified when we vary the parameters.

We specify the initial curvature perturbation by giving K as a function of r . However, both r and K are gauge-dependent quantities and so care is needed when transferring the initial perturbation profile onto the grid used for the numerical calculations. The Schwarzschild circumference coordinate R used in the code is invariantly defined and is related to r by $R_b = s(t)r$, where R_b is the homogeneous value of R at a co-moving location before introducing the perturbation. The particular values of $s(t)$ and r are gauge dependent, but what is important is that their product is invariantly defined. Another gauge invariant quantity is the product $K(r)r^2$. These two invariantly defined products are connected by the presence of the comoving coordinate in both of them and therefore a particular specification of one of these three variables will fix also the gauge of the others.

To do this we start by comparing at an initial time the length scale R_0 of the perturbation with respect the horizon scale

$$R_0 = NR_H, \quad (89)$$

where N is the number of horizon scales inside the scale of the perturbation. We need to choose N such that the perturbation length scale is much larger than the horizon scale and, from the definition of ϵ in (27), we have

$$\epsilon = \frac{1}{N^2}. \quad (90)$$

To have $\epsilon \ll 1$ we need to have $N \gg 1$ and N will be one of the input parameters used to impose the initial conditions. Expression (89) gives also a direct link between the scale factor and the value of r_0

$$s(t) = \frac{NR_H}{r_0}, \quad (91)$$

and we can use this to define the comoving coordinate as

$$r = \frac{R_b}{s(t)} = \frac{r_0}{NR_H}R_b \quad (92)$$

where the value of the circumferential coordinate R_b is calculated with equation (2), simply integrated for the background universe as

$$R_b = \left(\frac{\mu}{4\pi\rho} \right)^{1/3}. \quad (93)$$

Finally we need to find the value of r_0 to put into (91) and this is determined by condition (76) when the curvature profile is chosen.

To decide now how to parametrise $K(r)$ we start by making some physical considerations about what could be a reasonable perturbation shape. For a simple and natural description, it is useful to start with a centrally peaked profile of the energy density that looks similar to a Mexican hat profile, which means that outside the region of the overdensity there is an under-dense region that tends asymptotically to the flat solution. To describe an energy density profile with these properties one should choose a centrally peaked profile of curvature that tends asymptotically to zero with a suitable continuous function. The continuity should be ensured at least in the first and second derivatives, because these play a key role in the expressions for the perturbation profiles of the different variables. To conserve the common normalisation used in cosmology where a closed universe has a curvature equal to 1, we choose to normalise the curvature profile to have $K(0) = 1$, and then connect this point asymptotically to zero. This is of purely formal convenience however as the scaling is determined when fixing the gauge by comparison with invariantly defined quantities.

We start with a family of curvature profiles based on a Gaussian shape, described by

$$K(r) = \left(1 + \alpha \frac{r^2}{\Delta^2}\right) \exp\left(-\frac{r^2}{2\Delta^2}\right) \quad (94)$$

where α and Δ are two independent parameters. In the particular case $\alpha = 0$, $K(r)$ is exactly Gaussian. To understand the behaviour of this function as the parameters are varied we need to look at its first derivative given by

$$K'(r) = \frac{r}{\Delta^2} \left[\alpha - \left(1 + \alpha \frac{r^2}{\Delta^2}\right) \right] \exp\left(-\frac{r^2}{2\Delta^2}\right) \quad (95)$$

that we use to calculate the value of r_0 as function of α and Δ using (94) and (76). We find

$$\alpha x_0^2 - (5\alpha - 2)x_0 - 6 = 0, \quad \text{where} \quad x_0 \equiv \frac{r_0^2}{\Delta^2} \quad (96)$$

with the following solutions

$$r_0^2 = 3\Delta^2 \quad \text{if} \quad \alpha = 0 \quad (97)$$

$$r_0^2 = \Delta^2 \frac{(5\alpha - 2) \pm \sqrt{(5\alpha - 2)^2 + 24\alpha}}{2\alpha} \quad \text{if} \quad \alpha \neq 0 \quad (98)$$

If α is positive only the solution of (98) with the positive sign is acceptable because the other one gives r_0 being negative. If α is negative, both of the solutions are acceptable in these sense, and the one to associate with r_0 is the smaller one, which is anyway the one with the positive sign. The ratio $(r_0/\Delta)^2$ changes with α and its behaviour is plotted in Figure 1. From (97) and (98) we see that, for a given value of α , r_0 is a linear function of Δ .

The solution for r_0 can now be used in (92) to transform the spatial comoving coordinate in the background coordinate R_b .

$$\frac{r^2}{\Delta^2} = \frac{F(\alpha)}{2\alpha} Z^2, \quad \text{where} \quad Z \equiv \frac{R_b}{NR_H} \quad (99)$$

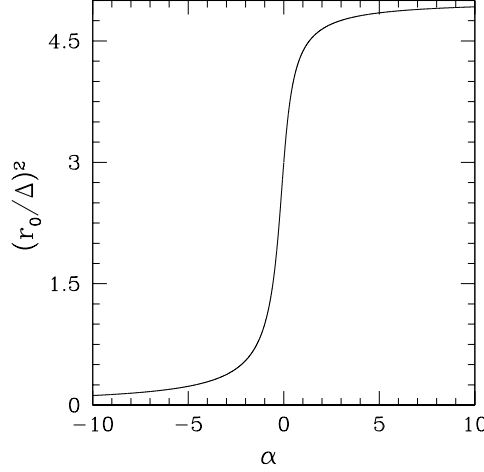


Figure 1. The behaviour of $(r_0/\Delta)^2$ with varying α .

and

$$F(\alpha) \equiv (5\alpha - 2) + \sqrt{(5\alpha - 2)^2 + 24\alpha} \quad \text{if } \alpha \neq 0 \quad (100)$$

$$\frac{F(\alpha)}{\alpha} = 3 \quad \text{if } \alpha = 0 \quad (101)$$

The variable Z is normalised with the length scale of the perturbation and therefore it is equal to 1 at the edge of the overdensity. One can notice that the parameter Δ cancels in the expression for r/r_0 in terms of Z , and this makes it simple to interpret the physical meaning of α and Δ . In fact if we write the energy density perturbation profile as function of Z we get

$$\begin{aligned} \tilde{e}(Z) = \Phi(\xi) \frac{\Delta^2}{2\alpha} F(\alpha) & \left[1 + \left(\frac{5}{6}\alpha - 1 \right) \frac{F(\alpha)}{2\alpha} Z^2 - \frac{\alpha}{2} \left(\frac{F(\alpha)}{2\alpha} \right)^2 Z^4 \right] \times \\ & \times \exp \left(-\frac{F(\alpha)}{4\alpha} Z^2 \right) \end{aligned} \quad (102)$$

and we see that the spatial profile given by the expression inside the parentheses is dependent only on α . The role of Δ , appearing only outside the brackets, is to parametrise the perturbation amplitude, increasing with increasing Δ . The separation of components in (102) is very useful from the practical point of view. It allows one to have complete control of the values of the input parameters, without a change in one of them affecting the other. For studying the curvature profiles, it is useful also to calculate the value of the second derivative of $K(r)$ at the centre, given by

$$K''(0) = \frac{\alpha - 1}{\Delta^2}, \quad (103)$$

and we see that when $\alpha > 1$ the value $K''(0)$ is positive and an off-centred peak appears in the profiles of both curvature and energy density. For $\alpha < 0$, instead, there is a second overdense region, corresponding to the second solution for r_0 found in (98). Because we are interested in solutions that represent perturbations centred

at $r = 0$ and behaving like a Mexican hat, we restrict our attention to the range of shapes given by $0 \leq \alpha \leq 1$.

In Figure 2 we have plotted corresponding curvature and energy density profiles for three different values of α between 0 and 1, taking the same value of Δ . The

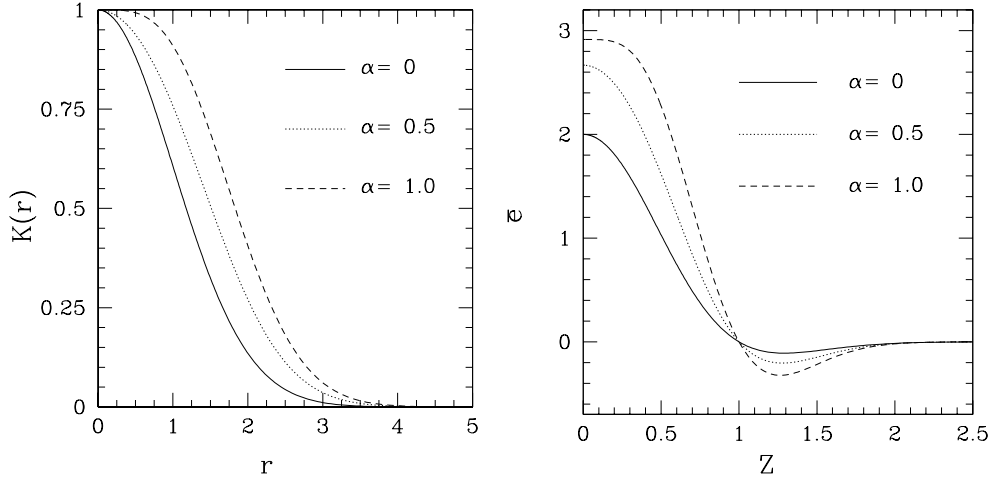


Figure 2. The left hand plot shows the curvature profile $K(r)$ as function of the comoving coordinate for three different value of α (0, 0.5 and 1). The right hand plot shows the corresponding profiles of energy density perturbation \tilde{e} plotted as functions of Z . These cases and those described in the next figures have been calculated with $\gamma = 1/3$ (equivalent to $\Phi = 2/3$.)

particular case of $\alpha = 0$ in (102) coincides with the Mexican hat shape used in [16, 22] in the radiation dominated epoch, where $\Phi = 2/3$:

$$\tilde{e}(Z) = \Delta^2 \left[1 + \frac{3}{2} Z^2 \right] \exp \left(-\frac{3}{2} Z^2 \right), \quad (104)$$

where the parameter Δ appears with the same meaning as the quantity used there to parametrise the perturbation amplitude.

A great advantage of this description is the possibility to calculate the perturbation amplitude δ defined in (77), directly from the curvature profile. For a general value of α (in the radiation epoch) this gives

$$\delta = \frac{1}{3N^2} \frac{\Delta^2}{\alpha} F(\alpha) \left(1 + \frac{F(\alpha)}{4} \right) \exp \left(-\frac{F(\alpha)}{4\alpha} \right). \quad (105)$$

Condition (73) should be taken into account to calculate the maximum allowed value of the perturbation amplitude for each shape. Therefore one needs to calculate the maximum value of Δ for each α and this is shown in Figure 3 for two different cases ($\alpha = 0$ and $\alpha = 1$). We can see clearly how an increment of Δ in the profile of $K(r)$ corresponds to an increment in the perturbation amplitude.

For completeness, we show in Figure 4 the behaviour for the two cases $\alpha > 1$ and $\alpha < 0$. The left hand panels show the behaviour of $K(r)$ while the right hand panels show the corresponding behaviour of $\tilde{e}(r)$. The top panels show cases with $\alpha > 1$ and

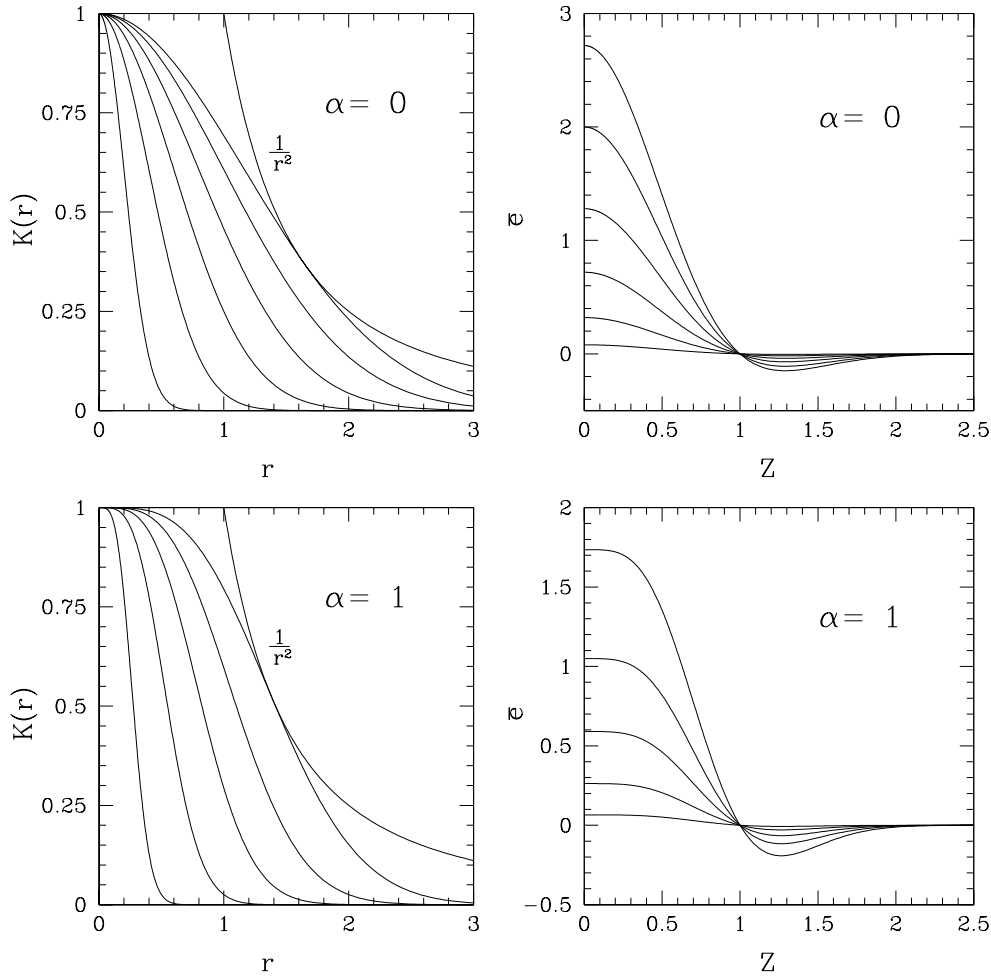


Figure 3. The left hand plots show the curvature profiles $K(r)$ as functions of the comoving coordinate r , while the right hand plots show the corresponding profiles for the energy density perturbation $\tilde{\epsilon}$ plotted as functions of Z . For $\alpha = 0$ (upper plots) the different profiles correspond to Δ between 0.2 and 1.1658, which is the maximum value allowed by (73). The values of Δ are higher for the higher curves. For $\alpha = 1$ (lower plots), the values of Δ used are between 0.15 and 0.77156.

we can see that increasing α enhances the off centred peak creating a kind of shell perturbation with spherical symmetry. The bottom panels show the behaviours of $K(r)$ and $\tilde{\epsilon}(r)$ for $\alpha < 0$ where the curvature profile is similar to a Mexican hat. This leads to the appearance of a new overdensity region outside the central perturbation, and the energy density profile tends asymptotically to the background from positive values, and not from negative ones as in the case of $\alpha \geq 0$. These types of profile are, of course, quite exotic and unlikely to happen, therefore we do not pay any more attention to them in the present work.

It is useful to consider also a different parametrisation of curvature that in some

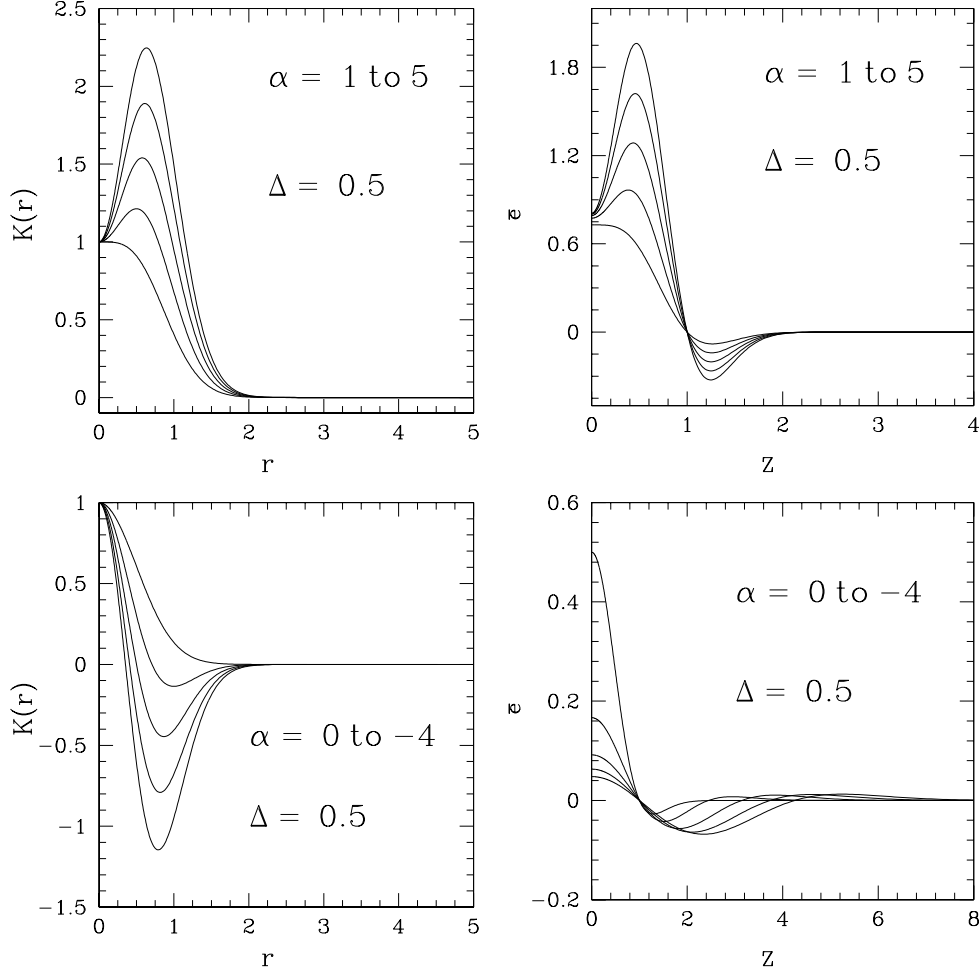


Figure 4. The left panel shows the behaviour of $K(r)$ for $\alpha \geq 1$ in the top row and for $\alpha \leq 0$ in the bottom row. The right panels show the corresponding behaviour of the energy density perturbation \bar{e} .

respects is similar to the one analysed until now in the range $0 \leq \alpha \leq 1$. We consider the following expression:

$$K(r) = \begin{cases} 1 & \text{if } r \leq \Delta_* \\ \left(1 + \frac{(r - \Delta_*)^2}{2\Delta^2}\right) \exp\left(-\frac{(r - \Delta_*)^2}{2\Delta^2}\right) & \text{if } r > \Delta_* \end{cases} \quad (106)$$

where the first derivative is

$$K'(r) = \begin{cases} 0 & \text{if } r \leq \Delta_* \\ -\frac{(r - \Delta_*)^3}{2\Delta^4} \exp\left(-\frac{(r - \Delta_*)^2}{2\Delta^2}\right) & \text{if } r > \Delta_* \end{cases} \quad (107)$$

In the left panel of figure 5 we show the behaviour of this new parametrisation of

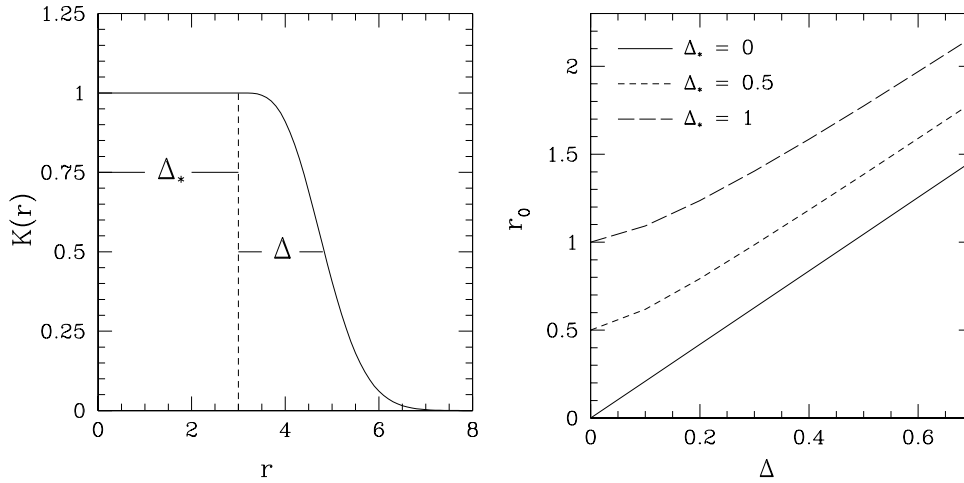


Figure 5. The left panel shows the general behaviour of $K(r)$ given by (106), indicating explicitly the meaning of the two parameters Δ and Δ_* . The right panel shows the value of r_0 with varying Δ , for three fixed values of Δ_* .

curvature showing explicitly the two different parameters Δ and Δ_* : Δ_* specifies the length of the plateau where $K(r) = 1$, while Δ gives the sharpness of the profile that connects the plateau to 0 at infinity. In the particular case of $\Delta_* = 0$ the curvature profile coincides with the previous case when $\alpha = 1$. Applying the condition given by (76) we obtain the equation to calculate the value of r_0 :

$$x_0^4 + \Delta_* x_0^3 - 3\Delta^2 x_0^2 - 6\Delta^4 = 0, \quad \text{where} \quad x_0 \equiv \frac{(r_0 - \Delta_*)^2}{2\Delta^2} \quad (108)$$

The analytical solution for x_0 in this case is complicated and so we have used the Newton-Rapson method to find the first positive root numerically. The behaviour of r_0 as function of Δ has been plotted in the right panel of Figure 5 for $\Delta_* = 0, 0.5, 1$ and we can see that the value of Δ_* represents the lower limit for r_0 when $\Delta = 0$, corresponding to a square wave curvature profile. Increasing Δ , the value of r_0 grows roughly linearly, in a similar way as in the previous formulation for a fixed value of α . The maximum value of Δ_* acceptable for the condition (73) is 1 when $\Delta = 0$, with the $1/r^2$ curve touching the corner of the square wave at $K(r_0) = 1$. The value of Δ_* , giving the length of the plateau, gives the minimum value of the perturbation amplitude δ , corresponding to $\Delta = 0$. The value of Δ is then specifying the sharpness of the perturbation similarly to α in the previous case.

In Figure 6 we show in the left top panel, how the profile of $K(r)$ is changing when Δ_* is constant and Δ is varying up until the limit given by (73), while in the left bottom panel we show how $k(r)$ behaves when Δ is constant and Δ_* is changing. In the right panels we show the corresponding behaviours of $\tilde{e}(r)$.

5. Numerical examples

In section 5.1 we make some numerical tests to calculate how small ϵ should be in order to make the linear approximation satisfactory. Then in section 5.2 we show

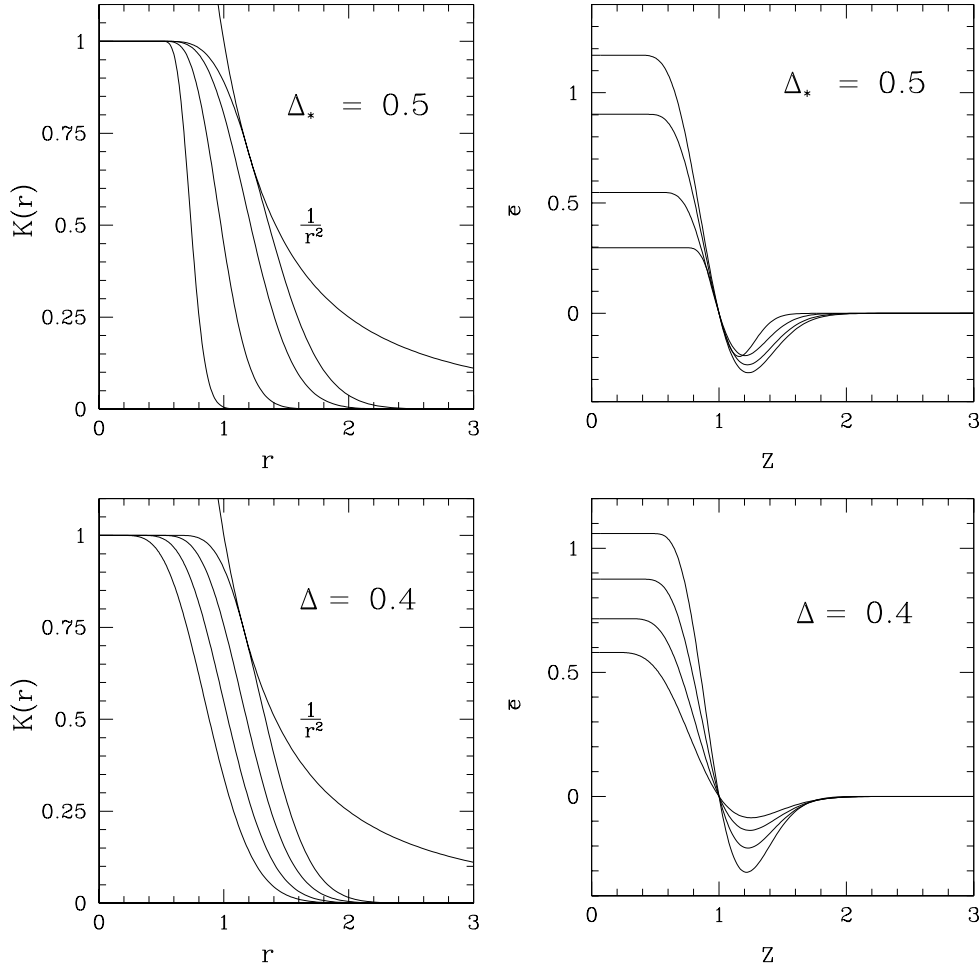


Figure 6. The left panels show the curvature profile $K(r)$ for Δ_* constant and varying Δ in the top row and for Δ constant and varying Δ_* in the bottom row. The corresponding behaviour of the energy density perturbation \tilde{e} is plotted in the right panels.

some explicit calculation for PBH formation, summarising the results in the phase space of parameters.

5.1. Numerical tests

Now we discuss the numerical tests that we have made in order to be confident that the perturbation profile $K(r)$ has been introduced consistently into the code. We need to study the approximation of imposing a perturbation with a length scale much larger than the horizon length, in order to determine when ϵ is small enough to make higher order terms negligible. One test is to use equation (41) to rederive $K(r)$ after calculating the initial conditions for the various quantities. This expression is valid when the higher order terms are negligible, therefore we expect to find some difference

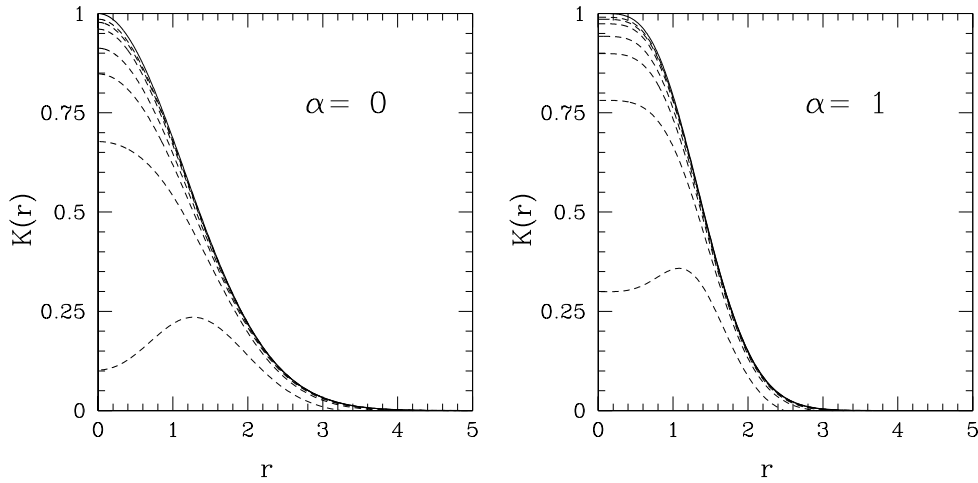


Figure 7. These plots show the comparison between the analytical (solid line) and the numerical (dashed lines) profiles of curvature given by (94). The different dashed lines correspond to $N = 1, 2, 3, 4, 6, 8, 10$ with the higher curves corresponding to the higher values of N . The profiles in the left hand plot are characterised by $(\alpha = 0, \Delta = 1.15)$, and the profiles in the right hand plot by $(\alpha = 1, \Delta = 0.77)$.

between the profile of $K(r)$ calculated with (41) and the original ones used to build the initial conditions. In Figure 7 and in the left panel of Figure 8 we plot the result of this test using both expressions for $K(r)$ with $\alpha = 0, \alpha = 1$ and $\Delta_* = 0.5$. In both cases a value of Δ very close to the maximum, corresponding to $K(r)r^2 = 1$, in order to make the test harder. The solid line is the analytical profiles of $K(r)$, while the dashed lines correspond to the derived profile of $K(r)$ with different values of N . The first value used was $N = 1$, that we know is not large enough as is also clear from the picture, and we then increase N progressively. We can appreciate the progressive approach to the analytical solution obtained in this way, where the most precise case shown in the plots corresponds to $N = 10$. The centre of the perturbation is the region where there is the largest difference because it corresponds to the part of the perturbation that is initially inside the horizon. It is therefore useful to quantify precisely the error in the centre of the perturbation and study how it varies with respect to N . (The difference between the values of the integrated δ will give a weaker estimate than this because their calculation takes into account also regions outside the horizon where the convergence is easier, as one can see from Figure 7 and Figure 8.)

In the right panel of Figure 8 the difference between the central values of the analytical and numerical solutions for $K(r)$ is plotted as a function of N . The white and black triangles differ in the value of α , while the black dots refer to $\Delta_* = 0.5$, and we can see clearly that the error is behaving like $\epsilon = 1/N^2$, represented by the dotted curve, with a slight difference between the different cases considered. This test is consistent with the scheme of the perturbative analysis that considers higher order terms behaving like ϵ^2 .

To be completely sure of the accuracy, we have done also one more test for

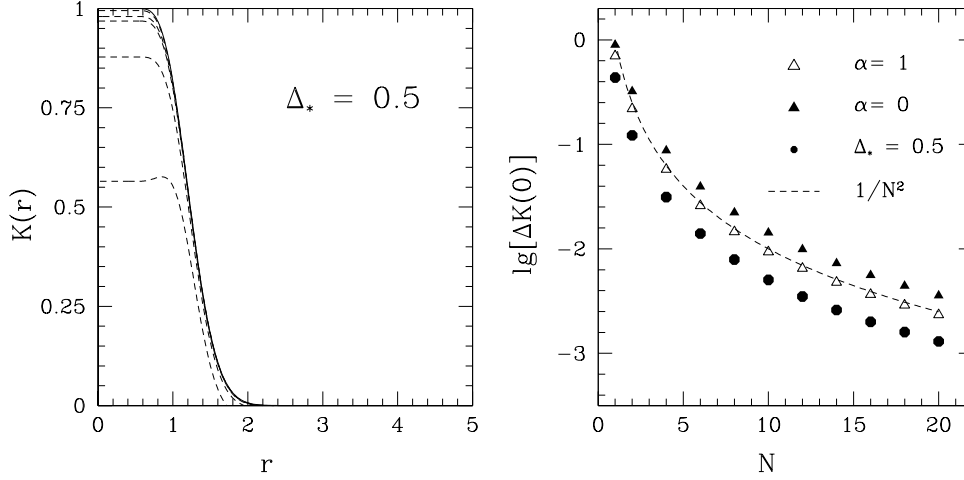


Figure 8. In the left panel we show the comparison between the analytical (solid line) and the numerical (dashed lines) profiles of curvature given by (106). The different dashed lines correspond to $N = 1, 2, 4, 5, 7, 10$ with the higher curves corresponding to the higher values of N . In the right panel we show the difference between the central value of the analytical and numerical profiles of $K(r)$ in Figure 7 and in the left panel, plotted as a function of N .

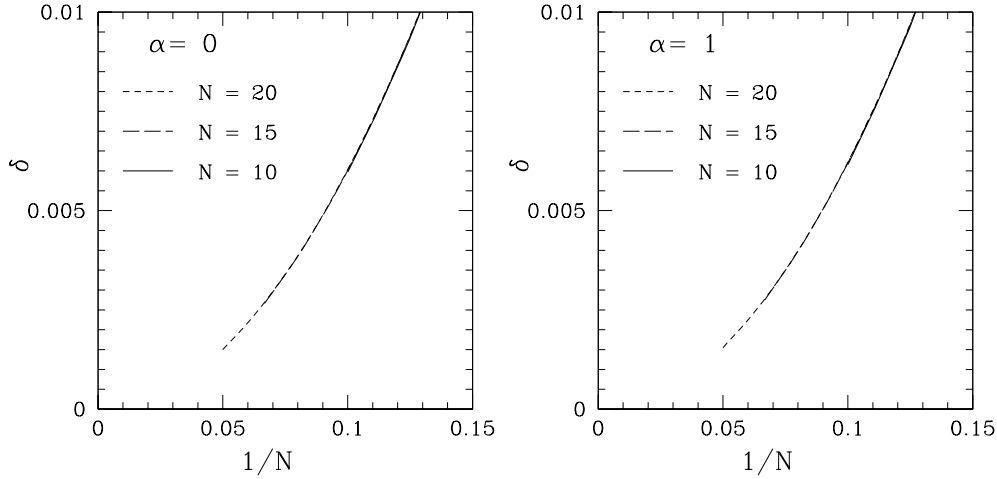


Figure 9. These plots show three time evolutions of δ calculated with the same profiles of $K(r)$ studied in figure 7 and 8; the three evolutions have different initial values of N .

the same $K(r)$, comparing the evolutions of a perturbation obtained with the same curvature profiles but using different initial values of N , and in Figure 9 we show the value of δ calculated during the evolution and plotted against $1/N$. It can be seen that there is no significant difference between $N = 10$ and $N = 20$, we therefore feel

confident in using a value of $N = 10$ to build the initial conditions with $K(r)$ given by (94), corresponding to an error of $\sim 1\%$ in the inner region. The test for $\alpha = 1$ corresponds also to the second formulation with $\Delta = 0$ and in this case too $N = 10$ is a satisfactory choice.

5.2. Description of the calculations

Calculations of black hole formations with these new initial conditions are very similar to those presented previously with the same numerical technique [22]. Therefore we show just a sample case in Figure 10, remembering that when using the observer-time slicing, black hole formation occurs when the lapse $f \rightarrow 0$ and $\Gamma + U \rightarrow 0$ together, (see [22]). The left hand plot shows the behaviour of $2M/R$ and we see the asymptotic approach to 1 of the maximum of this curve, that determines the exact location on the grid at which the apparent horizon is forming. The right hand plot shows the corresponding behaviour of the mass, as a function of R , giving value of the mass of the hole. In figure 10 the circumferential radius R and mass M have been normalised with respect to the values for the horizon scale at the horizon crossing time.

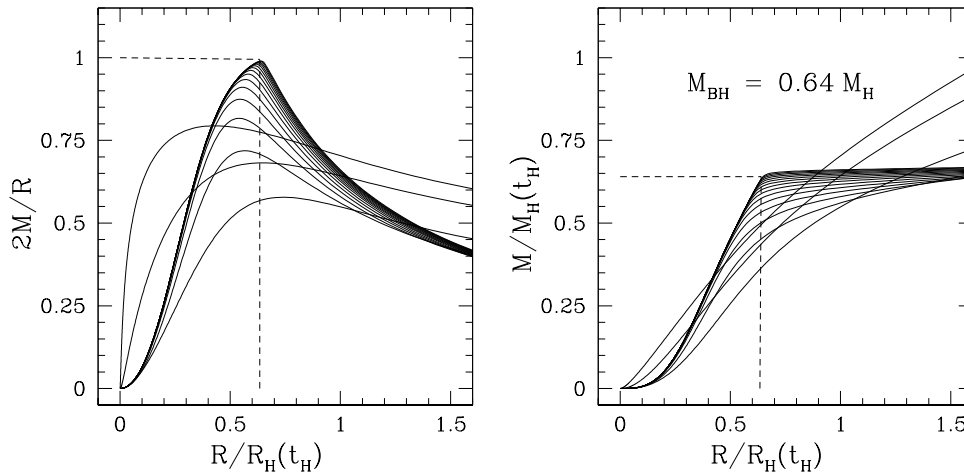


Figure 10. A typical evolution leading to black hole formation: the initial curvature profile used is characterised by $\alpha = 0$ and $\Delta = 1.02$, which give $(\tilde{\delta} - \tilde{\delta}_c) = 1.3 \times 10^{-2}$. The left-hand panel shows the profile of $2M/R$ at different times with the approach to 1 of the maximum value; the right-hand panel shows the corresponding evolution of the mass.

The only significant difference with respect to the earlier calculations [22] is that we have not seen any appearance of shock behaviour during the formation of black holes, for any of the parameters used so far. In the past Musco et al [22] were observing the formation of shocks when the amplitude of the perturbation was very close to the threshold δ_c for black hole formation ($(\delta - \delta_c) \lesssim 10^{-4}$). As we said earlier, the initial conditions with $\alpha = 0$ give the same Mexican hat shape of perturbation used in the previous calculations, and so it is plausible to think that the shock behaviour was caused by a small residual decaying mode component which was still present in the previous calculations but is avoided in the present ones.

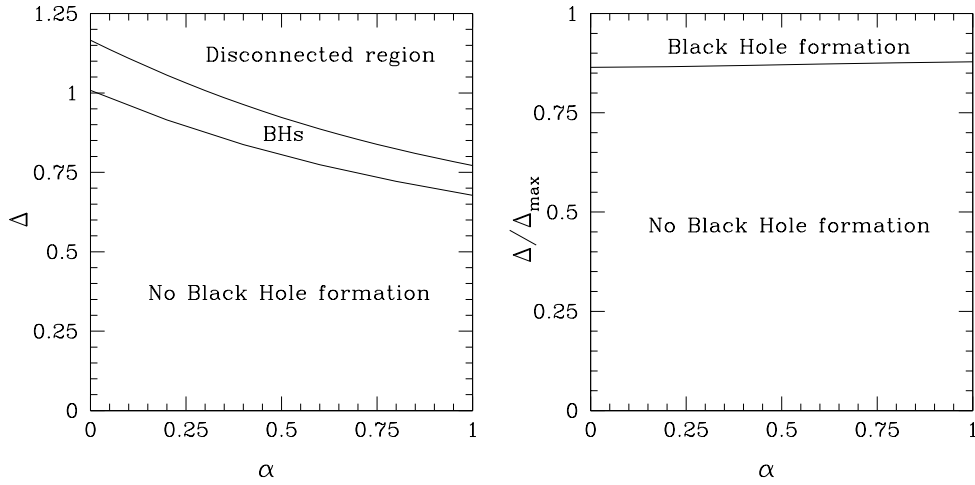


Figure 11. These plots show which values of α and Δ lead to black hole formation or, in the left panel, to an initial perturbation already disconnected from the rest of the Universe.

It is useful to introduce at this stage a measure of δ independent of the initial scale used to impose the initial conditions, in other words independent of the particular value of N used. Looking at expression (77), we can see that in the case of constant γ , if we define $\tilde{\delta} \equiv N^2\delta$, the expression becomes time independent, giving in the radiation epoch

$$\tilde{\delta} = \frac{2}{3}K(r_0)r_0^2. \quad (109)$$

Comparing this value with the value of δ at horizon crossing, we find that it is of the same order (with a small correction due to the non linear growth near to the horizon crossing). We therefore use $\tilde{\delta}$ to characterise the amplitude of a perturbation for the rest of the discussion.

The most important result of this calculation is in establishing the parameter ranges giving black hole formation. Using the first curvature formulation, what we did in practice was to fix successive particular values of α and find the corresponding threshold values of Δ . In Figure 11 we see a synthesis of these calculations. The left hand panel shows the results obtained for each value of Δ and α used in parametrisation (94), and this divides the plane into three different regions: the first corresponding to no black hole formation, the second to black hole formation and the third to a disconnected initial perturbation ($K(r)r^2 \geq 1$). The right hand panel shows the same results but with Δ normalised with respect to the maximum value Δ_{\max} , corresponding to the boundary of the third region of the plane. In both ways of presenting this, we see that the range of parameters leading black-hole formation is narrow with respect the range of no black hole formation, and this shows that black hole formation is difficult to achieve, needing an amplitude of the perturbation near to the maximum value.

The same results are shown also plotting $\tilde{\delta}$ with respect to α in Figure 12. This shows an interesting feature that is the small change in $\tilde{\delta}_c$ and $\tilde{\delta}_{\max}$ when the shape of perturbation changes with changing α . We have found $\tilde{\delta}_c \simeq 0.45$ and $\tilde{\delta}_{\max} \simeq 0.60$

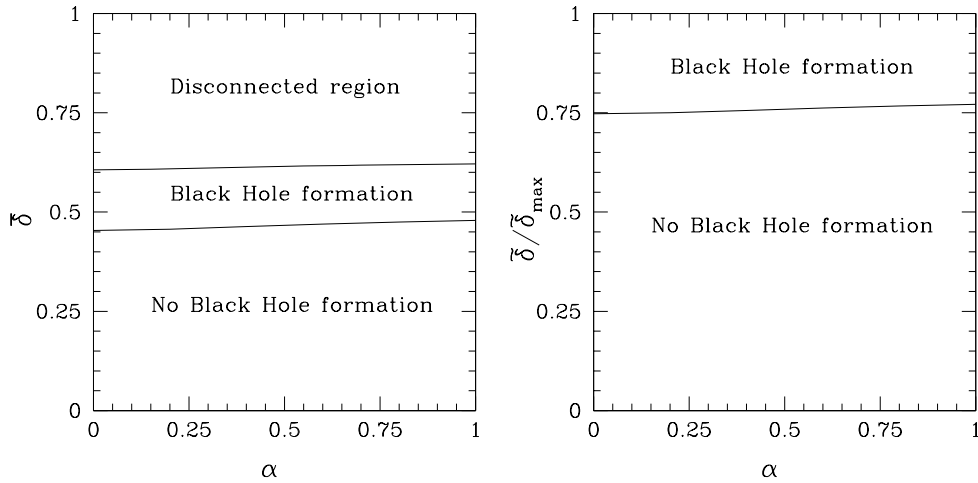


Figure 12. These plots show how $\tilde{\delta}_c$, the threshold amplitude for black hole formation, varies with α . The left panel also shows when the value of $\tilde{\delta}$ is able to disconnect the perturbation from the rest of the Universe.

for $\alpha = 0$ and $\tilde{\delta}_c \simeq 0.47$ and $\tilde{\delta}_{\max} \simeq 0.62$ for $\alpha = 1$. This is consistent with figure 11, where the increasing of α is balanced by the decreasing of the threshold value of Δ , making the final values of $\tilde{\delta}_c$ and $\tilde{\delta}_{\max}$ almost unchanged. The value of $\tilde{\delta}_c$ found is consistent with the result of [22], where $\delta_c \simeq 0.43$ at horizon crossing for a Mexican-hat profile. The slight difference occurs just because of the difference between $\tilde{\delta}_c$ and δ_c calculated at the horizon crossing time.

We can see this behaviour looking also at figure 13 where the variation of the curvature and energy density profiles for the different threshold solutions is plotted. For the curvature we see that there is a region where the values of $K(r)$ for different values of α are nearly the same and this corresponds, in fact, to the location of r_0 . The energy density profile shows that the difference is just in the shape of the central part, with almost the same profile for $Z \gtrsim 0.5$.

We can so conclude that the variations in the parametrisation of curvature given by (94) have not played a large role in the determination of the threshold amplitude $\tilde{\delta}_c$ for black hole formation. This conclusion is however not definitive because we need to compare the results obtained from different expressions for $K(r)$ in order to really understand how strongly the threshold for black hole formation is dependent on the initial perturbation shape.

In Figure 14 we show the parameter space for the second curvature parametrisation given by (106). In the left panel we show the parameter space for Δ and Δ_* , and we see the three different regions of no black hole, black hole formation and disconnected perturbation seen also in Figure 11. In the right panel we plot the same results using the parameters Δ_* and $\tilde{\delta}$ calculated with (109), and in this case we have a region of parameters that is mathematically forbidden from the definition (109). The reason is due to the minimum value of r_0 given by Δ_* (see right panel of figure 5), and the curve that corresponds to the boundary of the forbidden region is given by $\tilde{\delta} = 2/3 \Delta_*^2$. Equation (109) also shows that the maximum value of the “disconnected region condition” is when $K(r_0)r_0^2 = 1$, and this is exactly the value corresponding to

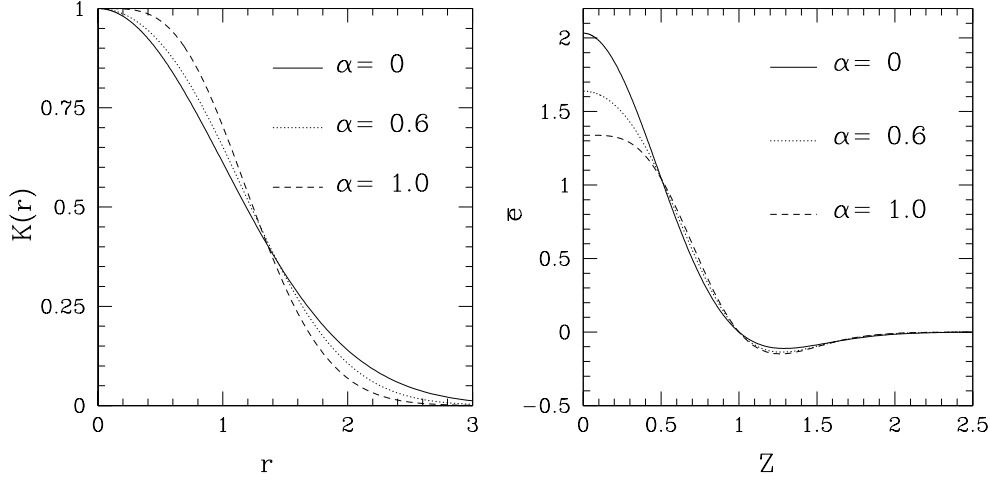


Figure 13. These plots show the curvature and energy density profiles corresponding to the threshold solutions for black hole formation, where the different lines correspond to different values of α .

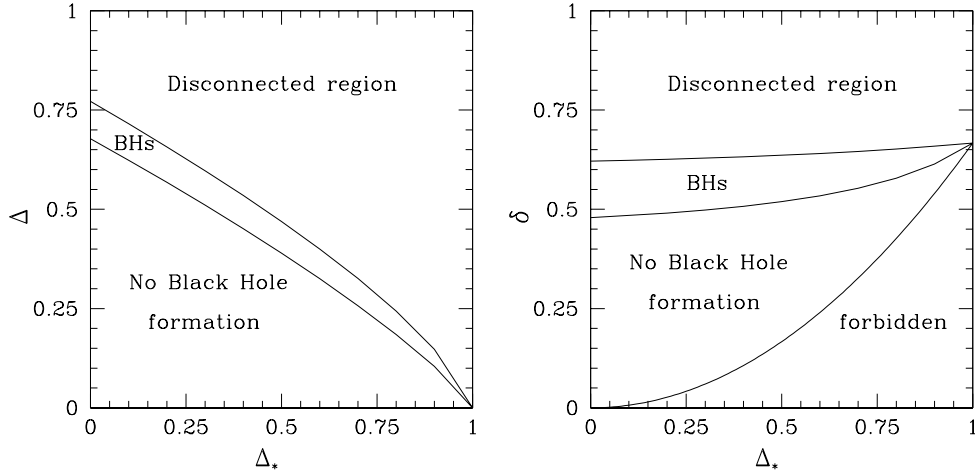


Figure 14. These plots show the range of parameters Δ , Δ_* , $\bar{\delta}$ referred to $K(r)$ given by (106) that gives origin to black hole formation.

the edge of the right plot where $\Delta_* = 1$. The curve given by $\bar{\delta} = 2/3 \Delta_*^2$ corresponds to square-wave perturbations. In general we can see that, when the profile is very sharp (corresponding to Δ being small), the formation of black holes is more difficult, until the limit of square-wave perturbations that never give black hole formation.

It is clear that the choice of perturbation shape significantly affects the results as regards the possibility for having black hole formation and should be made on the basis of physical considerations. Another important aspect is that we have observed no formation of shocks during black hole formation, for all of the range of parameters that we have explored. We suspect that this is a general feature for PBH formation

from purely growing mode initial conditions, and that the strong shock formation observed in the past [32] was connected with the presence of a non-linear decaying mode component in the initial conditions.

6. Conclusion

We have presented results for PBH formation where the problem of imposing initial conditions has been reformulated introducing a time independent curvature profile as the unique perturbation source. This corresponds to specify the initial conditions using a quasi homogeneous solution, that correspond to adiabatic perturbations that behaves in this regime as pure growing modes. We have calculated analytically the whole solution of the Misner - Sharp system of equations expressing all of the physical quantities in terms of the curvature profile $K(r)$, showing how the solution can be applied for the general case of γ being time dependent, which is useful for describing the Universe when it consists of different components. Studying the physical properties of the curvature profile we have shown that the perturbation amplitude δ is directly related to $K(r)$ and this allows to calculate easily the “closed universe” condition corresponding to have the perturbation defined in a region of the Universe topologically disconnected from the outer medium. We have then shown how the curvature profile $K(r)$ is linked to the curvature perturbation \mathcal{R} used in the literature.

We have performed numerical calculations using $\gamma = 1/3$ to test the initial conditions and we have carefully studied two different parameterisations of $K(r)$, described with a family of two independent parameters. We have shown that, to introduce consistently the new formulation of the initial conditions in the numerical scheme, the selection of a particular parametrisation of $K(r)$ implies to specify a consequent parametrisation of the comoving radius r and of the scale factor $s(t)$.

We think that specify the initial conditions using a curvature profile is a great improvement in the analysis of PBHs scenario because it allows to have a perfectly consistent link of the initial conditions to the power spectrum coming out from inflation, or any cosmological model. We have observed that, if the profile is sharper, the formation of PBHs is more difficult until the limit case of squared wave shape that never allows PBH formation. In the range of parameters that we have analysed the Gaussian curvature profile is the most favourable to produce black hole, with $\delta_c \simeq 0.45$ measured in the quasi homogeneous regime (see (109)), independently of the scale, while the squared wave shape gives $\delta_c = 2/3$, equal to the maximum value allowed from the “closed universe” condition. The comparison of results obtained from the two curvature parametrisation used shows that changing curvature parametrisation there are significant differences in the possibility of obtaining PBHs. This is an important reason to work out in the future the statistical connection between the possible parameterisations and the possible cosmological models, as inflation, obtaining constraints from PBHs on the different models.

Acknowledgements: In the course of this work, we have benefited from helpful discussions with many colleagues including John Miller, Bernard Carr, Marco Bruni, Luciano Rezzolla, Andrew Liddle and Carlo Baccigalupi.

Appendix A. Ricci Scalar calculations

The general spherically symmetric metric in the cosmic time coordinate is

$$ds^2 = -a^2 dt^2 + b^2 dr^2 + R^2 d\Omega^2 \quad (\text{A.1})$$

where the the metric tensor $g_{\alpha\beta}$ is diagonal and a , b and R are, in general, functions of r and t . The Christoffel symbols are calculated by

$$\Gamma_{\beta\gamma}^\alpha = \frac{1}{2} g^{\alpha\alpha} \left(\frac{\partial g_{\beta\alpha}}{\partial x^\gamma} + \frac{\partial g_{\gamma\delta}}{\partial x^\beta} - \frac{\partial g_{\beta\gamma}}{\partial x^\delta} \right), \quad (\text{A.2})$$

while the components of the Ricci Tensor are given by

$$R_{\alpha\beta} = \Gamma_{\delta\gamma}^\gamma \Gamma_{\alpha\beta}^\delta - \Gamma_{\delta\beta}^\gamma \Gamma_{\alpha\gamma}^\delta + \frac{\partial \Gamma_{\alpha\beta}^\gamma}{\partial x^\gamma} - \frac{\partial \Gamma_{\alpha\gamma}^\gamma}{\partial x^\beta} \quad (\text{A.3})$$

and to calculate the Ricci scalar we need to take into account only the diagonal components $R_{\alpha\alpha}$.

In the background universe with the FRW metric the metric components are therefore

$$a = 1 \quad b = \frac{s(t)}{\sqrt{1 - Kr^2}} \quad R = s(t)r, \quad (\text{A.4})$$

where the curvature K is a constant equal to 0, ± 1 . The diagonal components of the Ricci tensor are

$$R_{00} = 3 \frac{\ddot{s}}{s} \quad (\text{A.5})$$

$$R_{11} = \frac{s\ddot{s} + 2\dot{s}^2 + 2K}{1 - Kr^2} \quad (\text{A.6})$$

$$R_{22} = (s\ddot{s} + 2\dot{s} + 2K) r^2 \quad (\text{A.7})$$

$$R_{33} = R_{22} \sin^2 \theta \quad (\text{A.8})$$

and these are used to calculate the scalar curvature

$$R = 6 \left(\frac{\ddot{s}}{s} + \frac{\dot{s}^2}{s^2} + \frac{K}{s^2} \right). \quad (\text{A.9})$$

While the three curvature is obtained by removing the terms with the time derivatives,

$$R^{(3)} = 6 \frac{K}{s^2}. \quad (\text{A.10})$$

In the general case of the metric given by (A.1), the diagonal components of the Ricci tensor are

$$\begin{aligned} R_{00} &= \frac{1}{a} \frac{\partial a}{\partial t} \left(\frac{1}{b} \frac{\partial b}{\partial t} + \frac{2}{R} \frac{\partial R}{\partial t} \right) + \frac{a}{b^2} \frac{\partial a}{\partial r} \left(\frac{2}{R} \frac{\partial R}{\partial r} - \frac{1}{b} \frac{\partial b}{\partial r} \right) + \\ &\quad + \frac{a}{b^2} \frac{\partial^2 a}{\partial r^2} - \frac{1}{b} \frac{\partial^2 b}{\partial t^2} - \frac{2}{R} \frac{\partial^2 R}{\partial t^2} \quad (\text{A.11}) \\ R_{11} &= \frac{b}{a^2} \frac{\partial b}{\partial t} \left(\frac{2}{R} \frac{\partial R}{\partial t} - \frac{1}{a} \frac{\partial a}{\partial t} \right) + \frac{1}{b} \frac{\partial b}{\partial r} \left(\frac{1}{a} \frac{\partial a}{\partial r} + \frac{2}{R} \frac{\partial R}{\partial r} \right) + \end{aligned}$$

$$+ \frac{b}{a^2} \frac{\partial^2 b}{\partial t^2} - \frac{1}{a} \frac{\partial^2 a}{\partial r^2} - \frac{2}{R} \frac{\partial^2 R}{\partial r^2} \quad (\text{A.12})$$

$$R_{22} = \frac{R}{a^2} \frac{\partial R}{\partial t} \left(\frac{1}{b} \frac{\partial b}{\partial t} - \frac{1}{a} \frac{\partial a}{\partial t} \right) + \frac{R}{b^2} \frac{\partial R}{\partial r} \left(\frac{1}{b} \frac{\partial b}{\partial r} - \frac{1}{a} \frac{\partial a}{\partial r} \right) + \\ + \left(\frac{1}{a} \frac{\partial R}{\partial t} \right)^2 - \left(\frac{1}{b} \frac{\partial R}{\partial r} \right)^2 + R \left(\frac{1}{a^2} \frac{\partial^2 R}{\partial t^2} - \frac{1}{b^2} \frac{\partial^2 R}{\partial r^2} \right) + 1 \quad (\text{A.13})$$

$$R_{33} = R_{22} \sin^2 \theta \quad (\text{A.14})$$

To write the scalar curvature it is useful to define the following operators:

$$D_t \equiv \frac{1}{a} \frac{\partial}{\partial t}, \quad D_t^2 \equiv \frac{1}{a^2} \frac{\partial^2}{\partial t^2}, \quad D_r \equiv \frac{1}{b} \frac{\partial}{\partial r}, \quad D_r^2 \equiv \frac{1}{b^2} \frac{\partial^2}{\partial r^2} \quad (\text{A.15})$$

We then get

$$R = 2 \left[\frac{D_t^2 b}{b} + 2 \frac{D_t^2 R}{R} - \frac{D_r^2 a}{a} - 2 \frac{D_r^2 R}{R} + \left(\frac{D_t R}{R} \right)^2 - \left(\frac{D_r R}{R} \right)^2 + 2 \frac{D_t b}{b} \frac{D_t R}{R} - \right. \\ \left. - 2 \frac{D_t a}{a} \frac{D_t R}{R} - \frac{D_t a}{a} \frac{D_t b}{b} + 2 \frac{D_r b}{b} \frac{D_r R}{R} + \frac{D_r a}{a} \frac{D_r b}{b} - 2 \frac{D_r a}{a} \frac{D_r R}{R} + \frac{1}{R^2} \right] \quad (\text{A.16})$$

and substituting the expressions for the coefficients a , b and R given by (30,32,33) and expressing $\tilde{a}, \tilde{b}, \tilde{R}$ in terms of $K(r)$, we get with the use also of (28), that the Ricci scalar is given by

$$R = \left[6 \frac{\ddot{s}}{s} \left(1 + \epsilon \frac{3\gamma - 1}{5 + 3\gamma} \mathcal{K} \right) + \frac{\dot{s}^2}{s^2} \left(1 - \epsilon \frac{2(2 + 3\gamma)}{5 + 3\gamma} \mathcal{K} \right) + \frac{\mathcal{K}}{s^2} \right], \quad (\text{A.17})$$

where

$$\mathcal{K} = K(r) + \frac{r}{3} K'(r). \quad (\text{A.18})$$

It is useful to compare (A.17) with (A.9).

References

- [1] Zel'dovich Ya.B. & Novikov I.D. 1966 *Astron.Zh.* **43** 758 [*Sov.Astron.* **10** 602 (1967)]
- [2] Hawking S.W. 1971 *MNRAS* **152** 75
- [3] Carr B.J. 2003 *Lect. Notes Phys.* **631** 301
- [4] Hawking S.W. 1974 *Nature* **248** 30
- [5] Carr B.J. 1975 *Astrophys.J.* **201** 1
- [6] Nadezhin D.K., Novikov I.D. & Polnarev A. G. 1978 *Astron.Zh.* **55** 216 [*Sov.Astron.* **22(2)** 129 (1978)]
- [7] May M.M. & White R.H. 1966 *Phys.Rev.* **141** 1232
- [8] Pondurets M.A. 1964 *Astron.Zh.* **41** 1090 [*Sov.Astron.* **8** 868 (1965)]
- [9] Bicknell G.V. & Henriksen R. N. 1979 *Astrophys.J.* **232** 670
- [10] Green A.M. & Liddle A.R. 1997 *Phys.Rev.D* **56** 6166
- [11] Jedamzik K. & Niemeyer J.C. 1999 *Phys.Rev.D* **59** 124014
- [12] Khlopov M.Yu. & Polnarev A.G. 1980 *Phys.Lett.B* **97** 383
- [13] Polnarev A.G. & Zembroricz R. 1988 *Phys.Rev.D* **43** 1106
- [14] Crawford M. & Schramm D. N. 1982 *Nature* **298** 538
- [15] Niemeyer J.C. & Jedamzik K. 1998 *Phys.Rev.Lett* **80** 5481
- [16] Niemeyer J.C. & Jedamzik K. 1999 *Phys.Rev.D* **59** 124013
- [17] Choptuik M.W. 1993 *Phys. Rev. Lett.* **70** 9

- [18] Gundlach C. 1999 *Living Rev.Rel.* [<http://www.livingreviews.org/lrr-1999-4>]
- [19] Shibata M. & Sasaki M. 1999 *Phys.Rev.D* **60** 084002
- [20] Ivanov P. 1998 *Phys.Rev.D* **57** 7145
- [21] Green A.M., Liddle A.R. Malik K.A., Sasaki M. 2004 *Phys.Rev.D*, **70**, 041502
- [22] Musco I., Miller J.C., Rezzolla L. 2005 *Class. Quantum Grav.*, **22**, 1405
- [23] Misner C.W. & Sharp D.H. 1964 *Phys.Rev* **136** B571
- [24] Miller J.C. & Pantano O. 1990 *Phys.Rev.D* **42** 3334
- [25] Miller J.C. & Rezzolla L. 1995 *Phys.Rev.D* **51** 4017
- [26] Hernandez W.C. & Misner C.W. 1966 *Astrophys.J.* **143** 452
- [27] Liddle A.R. & Lyth D.H. 2000 *Cosmological Inflation and Large-Scale Structure* Cambridge University Press
- [28] Lifshits E.M. & Khalamnikov I.M. 1963 *Usp. Fiz. Nauk.* **80**, 391 [*Sov. Phys. Usp.* **6**, 496 (1964)]
- [29] Lyth D.H., Malik K.A., Sasaki M. 2005 *JCAP* **May** 004
- [30] Langlois D. & Vernizzi F. 2005 *Phys.Rev.Lett.* **95** 091303
- [31] Padmanabhan T. 1993 *Structure Formation in the Universe* Cambridge University Press
- [32] Hawke I. & Stewart J. M. 2002 *Class. Quantum Grav.* **19** 3687